Letter

Optical flux pump in the quantum Hall regime

Bin Cao,[1] Tobias Grass,[2] Glenn Solomon,[1] and Mohammad Hafezi[1,3]
[1]*Joint Quantum Institute, NIST/University of Maryland, College Park, Maryland 20742, USA*
[2]*ICFO-Institut de Ciencies Fotoniques, The Barcelona Institute of Science and Technology, Castelldefels (Barcelona) 08860, Spain*
[3]*IREAP, University of Maryland, College Park, Maryland 20742, USA*

(Received 19 April 2021; revised 7 June 2021; accepted 8 June 2021; published 28 June 2021)

A seminal *gedankenexperiment* by Laughlin describes the charge transport in quantum Hall systems *via* the pumping of flux. Here, we propose an optical scheme which probes and manipulates quantum Hall systems in a similar way: When light containing orbital angular momentum interacts with electronic Landau levels, it acts as a flux pump which radially moves the electrons through the sample. We investigate this effect for a graphene system with Corbino geometry and calculate the radial current in the absence of any electric potential bias. Remarkably, the current is robust against the disorder which is consistent with the lattice symmetry, and in the weak excitation limit, the current shows a power-law scaling with intensity characterized by the novel exponent 2/3.

DOI: 10.1103/PhysRevB.103.L241301

Introduction. Multipole transitions beyond the dipole approximation apply when the Bohr radius of the quantum state is larger or comparable to the excitation wavelength. This is rarely the case for atoms or quantum dots [1–6]. However, in the quantum Hall regime, wave functions can be extended to a length scale comparable to optical wavelengths [7–12], and the coherence is topologically protected against dephasing [10,13]. Consequently, multipole transitions become possible [14–17]. Specifically, if the optical field has an orbital angular momentum (OAM) [5,18], these transitions can transfer angular momentum from photons to electrons, and an interesting interplay between topological properties of electrons and photons may be observed [19–21]. Similar effects also exist in synthetic quantum Hall system made of Rydberg polaritons [22]. Outside the quantum Hall regime, *incoherent* multipole interactions between light and condensed-matter systems have been experimentally studied [23–27]; and many theoretical efforts have been performed [28–30]. However, there has been no observation of *coherent* multipole interaction with quantum Hall states, to the best of our knowledge. In this context, disorder may play an important role as it mixes eigenstates of angular momentum, but previous studies have largely ignored its effect [15–17].

Here, to observe such a topological interplay, we theoretically study the interaction between light with OAM and a graphene device with Corbino geometry in the quantum Hall regime, see Fig. 1(a). We focus on the radial dynamics of the electrons in LLs upon illumination of light with nonzero OAM and propose an OAM-induced photocurrent measurement. We solve the Bloch equations incorporating the optical coupling, acoustic phonon relaxation, potential disorders, effective boundaries, and Pauli blockade. In particular, we first consider an ideal system without disorder which simplifies to a translationally invariant model which can be analytically solved. This yields an expression for the OAM-induced current, which scales with pump intensity to the power of 2/3. Second, we take into account short- and long-range disorders and boundary effects without intervalley mixings and numerically solve the Bloch equations. The results show that a radial current is generated as a result of electrons moving outward or inward between orbitals upon absorbing a photon with OAM. The current's direction and amplitude is determined by the OAM of the light with respect to the magnetic field. Remarkably, this is similar to the Laughlin pump [31] where a magnetic flux induces a spectral flow of the electrons' OAM, whereas in our scheme the flux is replaced by a light beam with a phase winding. We find that the current is reduced for larger disorder strength. However, we can recover the current through applying a voltage bias. Finally, we show that the numerical simulated current matches the scalings predicted analytically.

Landau levels in graphene. The system considered is a Corbino-shape graphene device [32,33] under a strong out-of-plane magnetic-field B as shown in Fig. 1(a). The magnetic field quenches the kinetic energies of the electrons and their states manifest as LLs. Here we consider two LLs, the zeroth LL (LL_0) and the first LL (LL_1). Under an achievable high magnetic field of 15 T, for example, the frequency corresponding to the transition between the two LLs is around 35 THz which lies in the midinfared optical regime. In graphene, very few other transitions match the same energy due to the inharmonic level spacing, and only LL_0 to LL_1 is allowed when the Fermi level is set in between them. We refer to transitions between different LLs as interband, whereas those among orbitals inside a LL as intraband. We ignore carrier-carrier interaction since the timescales make the Coulomb interaction irrelevant as we will show later. Also, we limit our discussion to the K valley and ignore the spin degree of freedom. Without any disorder, the spinor wave functions for LL_0 and LL_1 in the K valley of graphene are given as [34],

$$\bar{\Psi}_{0,\bar{m}} = \begin{pmatrix} 0 \\ |0,\bar{m}\rangle \end{pmatrix}, \qquad \bar{\Psi}_{1,\bar{m}} = \frac{1}{\sqrt{2}} \begin{pmatrix} |0,\bar{m}\rangle \\ |1,\bar{m}\rangle \end{pmatrix}. \tag{1}$$

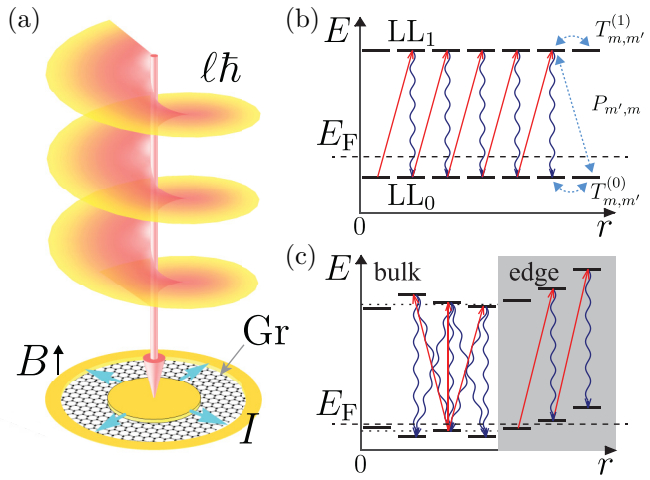

FIG. 1. (a) The illustration of the proposed setup. The Corbino-structured sample is concentric with the OAM beam. The OAM-induced current is measured between the inner and the outer electric contacts. (b) In a pristine system, the orbitals in each Landau level (LL) are degenerate in energy. The optical selection (red arrows) leads to an increase in OAM (for positive ℓ) and phonon relaxations (blue arrows) maintain the OAM. This equivalently leads to a directional transport of electrons. (c) In a system with disorder and confinement, the LLs are broadened in the bulk whereas the energy of the edge orbitals (shaded region) rises quickly. Only the edge states couple and relax pair wisely whereas the disordered bulk eigenstate may couple and relax to more than one eigenstate.

There are two quantum numbers for $\bar{\Psi}_{s,\bar{m}}$, the LL index $s \in \{0, 1\}$, and the orbital index $\bar{m} \in \mathbb{Z}^+$, which corresponds to OAM in the chosen symmetric gauge. In real space, each orbital $\Psi_{s,\bar{m}}$ looks like a circular ring [7], and the radius of the ring increases as $r_{\bar{m}} = \sqrt{2\bar{m}}l_c$, where l_c is the magnetic length. Without disorder, energies of these orbitals in each LL are degenerate as shown in Fig. 1(b).

To account for disorder, we include a disorder potential consistent with the symmetries of the lattice $V_{\rm dis} = \gamma[u_0(r,\theta)I + \mathbf{u}(r,\theta)\cdot\sigma]$ where γ is the strength of the disorder; $\gamma u_0(r,\theta)$ represents the long-range disorder arising from, e.g., charge impurities and $\gamma\mathbf{u}(r,\theta)$ is the short-range disorder associated with, e.g., defects, variations of sublattice potentials (u_z), and tunneling rates (u_x, u_y) [14,35]. Intervalley scatterings [36] are not considered in this valley-polarized model and corresponding intervalley effects may not be compatible. To account for boundary effects, we include a confinement potential $V_{\rm cf} = V_c\mathcal{H}(r - r_{\rm max})$, where $\mathcal{H}(\cdot)$ is the Heaviside step function. This modeling of confinement, without intervalley scattering, applies to, e.g., electrostatically defined edges [10,37] or zigzag edges [36]. We diagonalize the potential for LL_0 and LL_1 individually, and obtain the disordered LL eigenstates,

$$\Psi_{0,m} = \sum_{\bar{m}} c^m_{0,\bar{m}}\bar{\Psi}_{0,\bar{m}}, \qquad \Psi_{1,m} = \sum_{\bar{m}} c^m_{1,\bar{m}}\bar{\Psi}_{1,\bar{m}}. \tag{2}$$

Here we assume $\gamma \ll \delta$, where δ is the cyclotron energy (the LL gap), and, thus, the two LLs do not mix. Because of the disorder, m does not represent OAM anymore but numerates the orbitals with respect to their energy as the LL degeneracy has been lifted. We truncate our system size such that $m < m^*$, where m^* is the maximum index of the possibly occupied orbitals in our simulation, determined by the size of the sample through $r_{\rm max} = \sqrt{2m^*}l_c$ assuming that the coherence length is larger than the system size. With $V_{\rm dis}$ and $V_{\rm cf}$, the orbitals in the bulk will give rise to LL broadening, whereas the orbitals on the physical edges increase energy with m [Fig. 1(c)].

Light-matter interaction. We illuminate the sample with a laser beam which is in resonance with the interband transition between LL_0 and LL_1. The beam is concentric with the center of the sample and may contain a nonzero OAM as shown in Fig. 1(a). See Ref. [38] for the scenarios where the beam is partially blocked or shifted away from the center.

The light-matter interaction is obtained with the minimal coupling $\boldsymbol{p} \to \boldsymbol{p} - e\mathbf{A}$,

$$H_{\rm I}(t) = ev_{\rm F}\mathbf{A}(t)\cdot\sigma, \tag{3}$$

where $v_{\rm F}$ is the Fermi velocity, $\mathbf{A}(t)$ is the vector potential of light and it can be expressed as

$$\mathbf{A}(t) = \mathbf{A}_0(r,\theta)e^{-i\omega t} + \mathbf{A}_0^*(r,\theta)e^{i\omega t}, \tag{4}$$

$$\mathbf{A}_0(r,\theta) = A(r)e^{i\ell\theta}\mathbf{p}. \tag{5}$$

Here, $A(r)$ is the mode of the light, which can be the Bessel mode [39], or the Laguerre-Gauss mode [5]; $\mathbf{p}$ is the in-plane polarization of the field. The twisted phase term $e^{i\ell\theta}$ represents the OAM carried by the light, and ℓ counts the OAM.

In the interaction picture, i.e., after a unitary transformation which describes the system in a rotating frame with frequency ω, the time dependence is removed from the Hamiltonian, and we have the light-matter interaction Hamiltonian in graphene as $H_{\rm I} = ev_{\rm F}A(r)(e^{i\ell\theta}\sigma_- + e^{-i\ell\theta}\sigma_+)$ where we assume that the field is right-circular polarized, i.e., $\mathbf{p} = \mathbf{p}_+$. Only the off-diagonal terms are nonzero, and they correspond to interband optical transitions between LL_0 and LL_1 [38].

Bloch equations. We define the annihilation and creation operators a_m, $a_m^\dagger$ for electrons in orbital m in LL_0, and b_m, $b_m^\dagger$ for LL_1. They satisfy $\{a_m, a_{m'}^\dagger\} = \{b_m, b_{m'}^\dagger\} = \delta_{m,m'}$. We can rewrite the light-matter interaction as

$$H_{\rm I} = \sum_{m,m'} \Omega_{m',m}b_{m'}^\dagger a_m + \Omega_{m',m}^* a_m^\dagger b_{m'}. \tag{6}$$

The Rabi frequency for each pair of orbitals is obtained as $\Omega_{m',m} = \langle\Psi_{0,m}|H_{\rm I}|\Psi_{1,m'}\rangle$. It takes nonzero values only for interband couplings between LL_0 and LL_1, but there is no optical couplings between orbitals inside the same LL. Without disorder, m coincides with the OAM of the orbital, and $\Omega_{m',m} = \Omega_0(\ell)\delta_{m',m+\ell}$. With disorder, this still holds approximately for edge states but not in the bulk where arbitrary orbitals can be coupled.

The Hamiltonian for the LLs in graphene reads $H_{\rm el} = \sum_m \mu_m^{(0)}a_m^\dagger a_m + \mu_m^{(1)}b_m^\dagger b_m$. Here $\mu_m^{(0)}$ and $\mu_m^{(1)}$ are the energies of orbitals in LL_0 and LL_1, respectively. The total Hamiltonian is given as $H = H_{\rm el} + H_{\rm I}$. We define the interband polarization as $P_{m,m'} = \langle a_{m'}^\dagger b_m\rangle$ and intraband polarizations as $T^{(0)}_{m,m'} = \langle a_{m'}^\dagger a_m\rangle$ for LL_0, $T^{(1)}_{m,m'} = \langle b_{m'}^\dagger b_m\rangle$ for LL_1 as illustrated in Fig. 1(b). When $m = m'$, the intraband polarization equals the occupation $T^{(0/1)}_{m,m} = \rho_m^{(0/1)}$.

From the Heisenberg equation of motion, we derive the coupled Bloch equations: for intraband polarizations of LL_0,

$$\dot{T}^{(0)}_{n,n'} = i\Delta^{(0)}_{n',n}T^{(0)}_{n,n'} + S^{(0)}_n(1-\rho^{(0)}_n)\delta_{n,n'} + i\sum_m(\Omega_{m,n'}P^*_{m,n} - \Omega^*_{m,n}P_{m,n'}), \quad (7)$$

for intraband polarizations of LL_1,

$$\dot{T}^{(1)}_{n,n'} = i\Delta^{(1)}_{n',n}T^{(1)}_{n,n'} - S^{(1)}_n\rho^{(1)}_n\delta_{n,n'} - i\sum_m(\Omega_{n,m}P^*_{n',m} - \Omega^*_{n',m}P_{n,m}), \quad (8)$$

for interband polarizations,

$$\dot{P}_{n,n'} = -i\Delta_{n,n'}P_{n,n'} - D\frac{1}{2}(S^{(0)}_{n'} + S^{(1)}_n)P_{n,n'} - i\sum_m\left(\Omega_{n,m}T^{(0)}_{m,n'} - \Omega_{m,n'}T^{(1)}_{n,m}\right), \quad (9)$$

within the rotating frame with respect to the laser frequency ω, $\Delta^{(s)}_{n,n'} = \epsilon_{sn} - \epsilon_{sn'}$, and $\Delta_{n,n'} = \epsilon_{1n} - \Delta - \epsilon_{0n'}$. We choose $D = 10$ to make the dephasing of the coherence much faster than the decay occupation lifetimes [38,40].

We also include interband acoustic phonon relaxation [40–42]. In Eqs. (7)–(9), $S^{(0)}_n$, $S^{(1)}_n$ are the scatter-in rate for LL_0 and scatter-out rates for LL_1, respectively: $S^{(0)}_n = \sum_{n'}\Gamma_{n,n'}\rho^{(1)}_{n'}$ and $S^{(1)}_n = \sum_{n'}\Gamma_{n',n}(1-\rho^{(0)}_{n'})$; $\Gamma_{n,n'}$ is the interband-polarization relaxation rate. The average relaxation time follows as $\tau = 1/\langle\Gamma_{n,n'}\rangle$. See Ref. [38] for modeling details of the relaxation.

Other relaxation mechanisms are not relevant in our case. For optical phonons in graphene, they are off-resonant with the energy gap. For Coulomb scatterings, we only excite carriers between the two lowest LLs, and other levels are either completely filled or empty, so Coulomb scattering is much slower than phonon scattering. Depending on the substrate, Coulomb scattering may become even slower due to screening.

Average radial position and the OAM-induced current. Without disorder and confinement, and with initial polarizations set to zero, the Bloch equations, Eqs. (7)–(9), reduce to a set of independent two-level systems. Their exact solution yields a compact expression for the current in the weak excitation limit,

$$I_r(\ell) = e\left(\frac{4|\Omega_0(\ell)|^4}{D^2\Gamma}\right)^{1/3}. \quad (10)$$

This is the maximum current one may get without disorder. Notably, it shows a novel scaling power of 1/3, which is a result of the Boltzmann scattering [38,40,42–44]. For ℓ much smaller than the total number of orbitals considered, we can approximate $I_r(\ell) = I_r$, independent of ℓ. We use I_r as a reference scale in the following discussions.

Once we include disorder in the system, the Bloch equations are solved numerically, and we determine the current by evaluating the average radial position of electrons, $\langle r\rangle = Tr\{\hat{\rho}\hat{r}\}$. Semiclassically, we define the average current as $I = \sqrt{m^*}\frac{e}{l_c}\frac{d\langle r\rangle}{dt}$. The factor $\sqrt{m^*}$ takes into account the circumference of the outer edge [38].

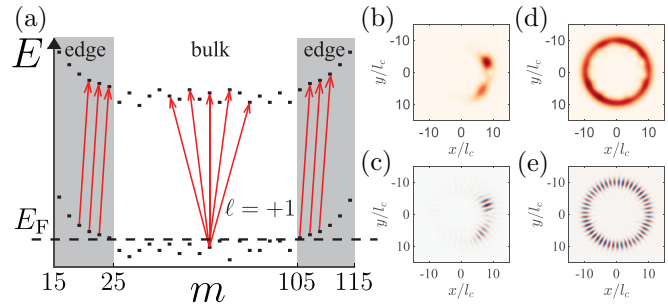

FIG. 2. (a) We illustrate the model used in the simulation. In total 100 orbitals are considered. The confinement is chosen such that 80 are bulk states whereas ten are outer edge states and ten are inner edge states. At $t = 0$, the bulk states in LL_0 are filled below the Fermi level E_F, whereas others are empty. We use $\ell = +1$ to illustrate the optical selection rules. In the bulk, states can couple to many others, whereas on the edge only the states with OAM difference equal to ℓ are strongly coupled. (b) The wave function of a bulk state in real space is shown. The bulk state is localized, and the phase of the wave function is disordered as shown in (c). (d) The edge state is delocalized, and the twisted phase of the wave-function (e) shows a well-defined OAM.

Results. In the simulation, we consider $m^* = 100$ orbitals in each LL [Fig. 2(a)]. In these orbitals, 80 of them are affected by the disorder in the bulk [Figs. 2(b) and 2(c)] and become localized, whereas the ten remain delocalized [Figs. 2(d) and 2(e)] on the outer edge, and the other ten are delocalized on the inner edge. We set the Fermi energy such that initially the 80 orbitals in the bulk are filled whereas the others are empty. We vary the average relaxation time τ from 50 fs to 10 ps [45]. For the light beam, we choose the vortex to be located in the hole of the Corbino disk such that on the disk the intensity profile can be assumed to be homogeneous $A(r) = A_0$. In fact, spatial variations of the intensity profile away from the vortex do not affect the results. The vector potential is represented as $|A_0| = E_0/\omega$. Here, the electric field is chosen as $E_0 = 8.50 \times 10^5$ V/m which is accessible experimentally.

We turn on the continuous-wave laser and solve the Bloch equations of the system Eqs. (7)–(9) to obtain the single-particle density matrix $\hat{\rho}$ as a function of time. The average relaxation rate of electrons between LLs in graphene can vary depending on the magnetic field [45,46]. For $\tau = 10$ ps, we observe Rabi oscillations for different ℓ's as shown in Fig. 3(a) where the occupation of LL_1 is plotted as a function of time. These oscillations are quickly damped, which can be understood as a result of optically induced diffusion. Specifically, light with OAM couples to orbitals which are distant from each other, and, therefore, electrons diffuse with OAM excitation. Since orbitals have different couplings strength due to a random disorder, they have inhomogeneous Rabi frequencies. While electrons diffuse into disordered states, the number of the Rabi frequencies participating increases, and, therefore, the total oscillation is damped. For $\tau = 50$ fs, we do not see significant Rabi oscillations as shown in Fig. 3(b) because of the faster relaxation compared to the Rabi frequency.

We evaluate the observables $\langle r\rangle$ and I as a function of time. In Fig. 3(c), we plot the average position of the 80 electrons

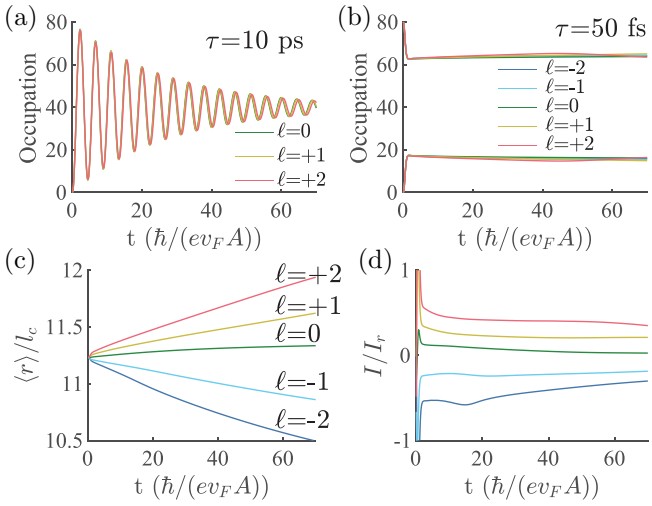

FIG. 3. (a) We plot the occupation of LL_1 as a function of time for different ℓ's. We observe Rabi oscillations which are damped. (b) For the average relaxation time $\tau = 50$ fs, one does not see Rabi oscillation because of the fast relaxation compared to the Rabi frequency. (c) The average radial position of electrons as a function of time for various OAM excitations for $\tau = 50$ fs. (d) The semiclassical current corresponding to (c) for various OAM excitations.

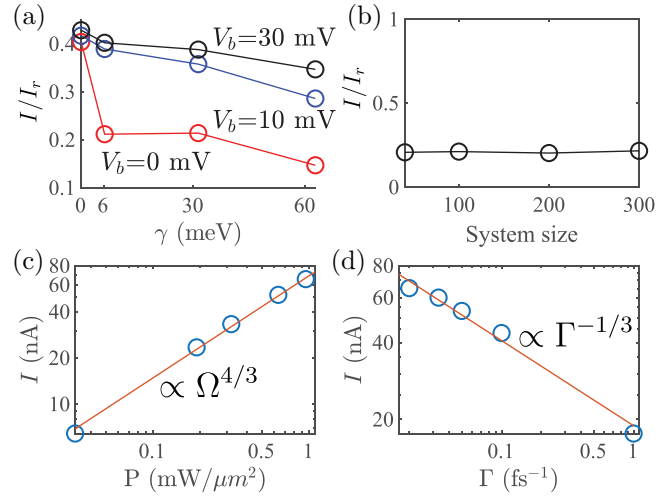

FIG. 4. (a) We plot the average current as a function of disorder strength γ with various bias voltages $V_b = 0, 10, 30$ mV. Increasing γ leads to a decrease in the average current. We apply a DC voltage bias V_b across the sample to recover the current. We find a bias increases the average current. Here we use $\ell = +1$, $\tau = 50$ fs. (b) We plot the average current for OAM $= +1$, $\tau = 50$ fs as a function of total number of orbitals (system size) considered in the simulation. The average current stays constant. (c) We plot the simulated current I as a function of pump intensity on log-log scales and compare with the reference current I_r multiplied by a constant 0.21 (orange line). (d) We plot the simulated I as a function of average relaxation rate $\Gamma = 1/\tau$ on log-log scales and compare with the reference current I_r multiplied by a constant 0.22 (orange line). The simulated results' scalings match very well with the analytical predictions.

as a function of time for excitations with different ℓ's. We find that for positive OAM, $\langle r \rangle$ increases with time, and larger OAM values lead to a faster increase. The resulting current is plotted in Fig. 3(d).

We average the current from Fig. 3(d) after it reaches equilibrium, and in Fig. 4(a) we plot this average as a function of disorder strength γ for OAM $= +1$ and $\tau = 50$ fs. It shows that larger disorder diminishes the OAM-induced current. This is expected because stronger disorder may introduce couplings between more disorder eigenstates and invalidate the pairwise selection rules of the orbitals. However, we can recover the current from disorder through a voltage bias.

Voltage biases control the system properties through the DC-Stark effect [47] or the Franz-Keldysh effect [40]. Here, we use a DC voltage to bias the two contacts of the sample and induce a DC current through the sample. Simplistically, this is equivalent to adding a potential gradient onto the radial direction of the sample [48–50]. Experimentally, the DC bias does not interfere with the OAM-induced current because one may chop the laser and make the OAM-induced current alternating. Then the alternating signal may be picked out by using a frequency-locked lock-in amplifier as a standard technique used in optoelectronics [51,52].

By having a small voltage bias across the Corbino sample, we can restore the rotational symmetry of the sample against disorders. In this way, the pairwise optical selection rules become valid again. As shown in Fig. 4(a), we plot the average current for voltage biases $V_b = 10, 30$ mV and without bias. Indeed, we see that voltage biases can recover the OAM-induced current.

In Fig. 4(b), we plot the average current as a function of the total number of orbitals considered in the simulation (system size). It shows that the OAM-induced current is independent of the system size. In this simulation it is assumed that the coherence length always exceeds the system size. Indeed, it has been demonstrated that the coherence length in graphene in the quantum Hall regime can be as long as several micrometers [9–12], comparable to the wavelength of the excitation.

Finally, we study the scaling of the OAM-induced current with pump intensity and relaxation. We have obtained an analytical expression for the current in Eq. (10) for a disorder-free system in the weak pumping regime. In Figs. 4(c) and 4(d), we plot the simulated OAM-induced current I for various pump intensities P and average relaxation times τ, respectively, in a disordered system. We compare with the scaling in Eq. (10), and they match very well. Therefore, the scaling of the OAM-induced current is not affected by the disordered bulk.

Discussion. We have proposed a measurement of the current resulting from the interactions between light with OAM and orbitals in LLs in graphene. We utilize the optical selection rules from the edge states, whose OAM is preserved due to the confinement potential, and adding a voltage bias extends the selection rules to even more states. The dynamics is an analogy to the Laughlin pump in the sense that flux insertion pumps charge through the system. In our scheme, however, this flux is added/removed by OAM of light through a nonadiabatic process rather than adiabatically by a magnetic field. We find a scaling of the current with pump intensity to the power of 2/3 as a result of Pauli blockade. This result, analytically obtained for the system without disorder, also holds for disordered systems as confirmed by numerical

simulations. This coherent interplay with vortex light provides new strategies to probe and manipulate the topology of matter.

Not limited to graphene, similar effects could also be seen in other systems, such as conventional two-dimensional electron gas [53] where neglecting of Coulomb interactions is better justified due to strong screenings. On the other hand, Coulomb interactions and dynamical screenings [54] may play an important role in other materials, such as transition metal dichalcogenide [55–57], and, therefore, in the future, it will be interesting to study how the OAM-induced current is affected by Coulomb interactions. Furthermore, this idea of OAM-included current might be useful in probing the topology of the fast-developing field of twistronics where correlated phases beyond LLs have been observed [58–60].

Acknowledgments. The work in Maryland was supported by Grants No. ARO W911NF2010232, No. ARL W911NF1920181, and No. AFOSR FA95502010223, the Simons Foundation, and the NSF funded PFC@JQI. T.G. acknowledges a fellowship granted by the "la Caixa" Foundation (Grant No. ID100010434, Fellowship Code No. LCF/BQ/PI19/11690013), and funding from Fundació Privada Cellex, Fundació Mir-Puig, Generalitat de Catalunya (AGAUR Grant No. 2017 SGR 1341, CERCA Program, QuantumCAT_U16-011424, co-funded by the ERDF Operational Program of Catalonia 2014-2020), Agencia Estatal de Investigación ("Severo Ochoa" Center of Excellence Grant No. CEX2019-000910-S, Plan National FIDEUA Grant No. PID2019-106901GB-I00/10.13039/501100011033, FPI), MINECO-EU QUANTERA MAQS [funded by State Research Agency (AEI) Grant No. PCI2019-111828-2/10.13039/501100011033], EU Horizon 2020 FET-OPEN OPTOLogic (Grant No. 899794), ERC AdG NOQIA, and the National Science Centre, Poland-Symfonia Grant No. 2016/20/W/ST4/00314.

[1] M. L. Andersen, S. Stobbe, A. S. Sørensen, and P. Lodahl, Strongly modified plasmon–matter interaction with mesoscopic quantum emitters, Nat. Phys. **7**, 215 (2011).

[2] C. T. Schmiegelow, J. Schulz, H. Kaufmann, T. Ruster, U. G. Poschinger, and F. Schmidt-Kaler, Transfer of optical orbital angular momentum to a bound electron, Nat. Commun. **7**, 12998 (2016).

[3] A. Afanasev, C. E. Carlson, C. T. Schmiegelow, J. Schulz, F. Schmidt-Kaler, and M. Solyanik, Experimental verification of position-dependent angular-momentum selection rules for absorption of twisted light by a bound electron, New J. Phys. **20**, 023032 (2018).

[4] G. De Ninno, J. Wätzel, P. R. Ribič, E. Allaria, M. Coreno, M. B. Danailov, C. David, A. Demidovich, M. Di Fraia, L. Giannessi *et al.*, Photoelectric effect with a twist, Nat. Photonics **14**, 554 (2020).

[5] L. Allen, M. W. Beijersbergen, R. J. C. Spreeuw, and J. P. Woerdman, Orbital angular momentum of light and the transformation of Laguerre-Gaussian laser modes, Phys. Rev. A **45**, 8185 (1992).

[6] S. Franke-Arnold, Optical angular momentum and atoms, Philos. Trans. R. Soc. A **375**, 20150435 (2017).

[7] B. E. Feldman, M. T. Randeria, A. Gyenis, F. Wu, H. Ji, R. J. Cava, A. H. MacDonald, and A. Yazdani, Observation of a nematic quantum Hall liquid on the surface of bismuth, Science **354**, 316 (2016).

[8] F. Ghahari, D. Walkup, C. Gutiérrez, J. F. Rodriguez-Nieva, Y. Zhao, J. Wyrick, F. D. Natterer, W. G. Cullen, K. Watanabe, T. Taniguchi *et al.*, An on/off Berry phase switch in circular graphene resonators, Science **356**, 845 (2017).

[9] C. Déprez, L. Veyrat, H. Vignaud, G. Nayak, K. Watanabe, T. Taniguchi, F. Gay, H. Sellier, and B. Sacépé, A tunable Fabry-Pérot quantum Hall interferometer in graphene, Nat. Nanotechnol. **16**, 555 (2021).

[10] Y. Ronen, T. Werkmeister, D. Najafabadi, A. T. Pierce, L. E. Anderson, Y. J. Shin, S. Y. Lee, Y. H. Lee, B. Johnson, K. Watanabe *et al.*, Aharonov Bohm effect in graphene Fabry Pérot quantum Hall interferometers, Nat. Nanotechnol. **16**, 563 (2021).

[11] D. S. Wei, T. van der Sar, J. D. Sanchez-Yamagishi, K. Watanabe, T. Taniguchi, P. Jarillo-Herrero, B. I. Halperin, and A. Yacoby, Mach-Zehnder interferometry using spin- and valley-polarized quantum Hall edge states in graphene, Sci. Adv. **3**, e1700600 (2017).

[12] S. M. Mills, A. Gura, K. Watanabe, T. Taniguchi, M. Dawber, D. V. Averin, and X. Du, Dirac fermion quantum Hall antidot in graphene, Phys. Rev. B **100**, 245130 (2019).

[13] Y. Zhang, Y.-W. Tan, H. L. Stormer, and P. Kim, Experimental observation of the quantum Hall effect and Berry's phase in graphene, Nature (London) **438**, 201 (2005).

[14] M. J. Gullans, J. M. Taylor, A. Imamoğlu, P. Ghaemi, and M. Hafezi, High-order multipole radiation from quantum Hall states in Dirac materials, Phys. Rev. B **95**, 235439 (2017).

[15] T. Graß, M. Gullans, P. Bienias, G. Zhu, A. Ghazaryan, P. Ghaemi, and M. Hafezi, Optical control over bulk excitations in fractional quantum Hall systems, Phys. Rev. B **98**, 155124 (2018).

[16] H. T. Takahashi, I. Proskurin, and J.-i. Kishine, Landau level spectroscopy by optical vortex beam, J. Phys. Soc. Jpn. **87**, 113703 (2018).

[17] H. T. Takahashi, I. Proskurin, and J.-i. Kishine, Selection rules for optical vortex absorption by Landau-quantized electrons, arXiv:1904.03083.

[18] S. Franke-Arnold, L. Allen, and M. Padgett, Advances in optical angular momentum, Laser Photonics Rev. **2**, 299 (2008).

[19] K. Y. Bliokh, P. Schattschneider, J. Verbeeck, and F. Nori, Electron Vortex Beams in A Magnetic Field: A New Twist on Landau Levels and Aharonov-Bohm States, Phys. Rev. X **2**, 041011 (2012).

[20] J. W. McIver, B. Schulte, F.-U. Stein, T. Matsuyama, G. Jotzu, G. Meier, and A. Cavalleri, Light-induced anomalous Hall effect in graphene, Nat. Phys. **16**, 38 (2020).

[21] H. Kim, H. Dehghani, H. Aoki, I. Martin, and M. Hafezi, Optical imprinting of superlattices in two-dimensional materials, Phys. Rev. Research **2**, 043004 (2020).

[22] P. A. Ivanov, F. Letscher, J. Simon, and M. Fleischhauer, Adiabatic flux insertion and growing of Laughlin states of cavity Rydberg polaritons, Phys. Rev. A **98**, 013847 (2018).

[23] Z. Ji, W. Liu, S. Krylyuk, X. Fan, Z. Zhang, A. Pan, L. Feng, A. Davydov, and R. Agarwal, Photocurrent detection of the orbital angular momentum of light, Science **368**, 763 (2020).

[24] S. Sederberg, F. Kong, F. Hufnagel, C. Zhang, E. Karimi, and P. B. Corkum, Vectorized optoelectronic control and metrology in a semiconductor, Nat. Photonics **14**, 680 (2020).

[25] K. B. Simbulan, T.-D. Huang, G.-H. Peng, F. Li, O. J. Gomez Sanchez, J.-D. Lin, J. Qi, S.-J. Cheng, T.-H. Lu, and Y.-W. Lan, Twisted-light-revealed lightlike exciton dispersion in monolayer MoS_2, arXiv:2001.01264.

[26] D. Sanvitto, F. Marchetti, M. Szymańska, G. Tosi, M. Baudisch, F. P. Laussy, D. Krizhanovskii, M. Skolnick, L. Marrucci, A. Lemaitre *et al.*, Persistent currents and quantized vortices in a polariton superfluid, Nat. Phys. **6**, 527 (2010).

[27] M.-S. Kwon, B. Y. Oh, S.-H. Gong, J.-H. Kim, H. K. Kang, S. Kang, J. D. Song, H. Choi, and Y.-H. Cho, Direct Transfer of Light's Orbital Angular Momentum Onto a Nonresonantly Excited Polariton Superfluid, Phys. Rev. Lett. **122**, 045302 (2019).

[28] G. F. Quinteiro and J. Berakdar, Electric currents induced by twisted light in quantum rings, Opt. Express **17**, 20465 (2009).

[29] M. B. Farias, G. F. Quinteiro, and P. I. Tamborenea, Photoexcitation of graphene with twisted light, Eur. Phys. J. B **86**, 432 (2013).

[30] J. Wätzel, A. Moskalenko, and J. Berakdar, Photovoltaic effect of light carrying orbital angular momentum on a semiconducting stripe, Opt. Express **20**, 27792 (2012).

[31] R. B. Laughlin, Quantized Hall conductivity in two dimensions, Phys. Rev. B **23**, 5632 (1981).

[32] Y. Zeng, J. I. A. Li, S. A. Dietrich, O. M. Ghosh, K. Watanabe, T. Taniguchi, J. Hone, and C. R. Dean, High-Quality Magnetotransport in Graphene using the Edge-Free Corbino Geometry, Phys. Rev. Lett. **122**, 137701 (2019).

[33] J. Li, Q. Shi, Y. Zeng, K. Watanabe, T. Taniguchi, J. Hone, and C. Dean, Pairing states of composite fermions in double-layer graphene, Nat. Phys. **15**, 898 (2019).

[34] M. O. Goerbig, Quantum Hall effects, arXiv:0909.1998.

[35] S. Das Sarma, S. Adam, E. H. Hwang, and E. Rossi, Electronic transport in two-dimensional graphene, Rev. Mod. Phys. **83**, 407 (2011).

[36] C. W. J. Beenakker, Colloquium: Andreev reflection and Klein tunneling in graphene, Rev. Mod. Phys. **80**, 1337 (2008).

[37] J. Li, R.-X. Zhang, Z. Yin, J. Zhang, K. Watanabe, T. Taniguchi, C. Liu, and J. Zhu, A valley valve and electron beam splitter, Science **362**, 1149 (2018).

[38] See Supplemental Material at http://link.aps.org/supplemental/10.1103/PhysRevB.103.L241301 for details. The Supplemental Material includes references to Refs. [24,34,41,42,61–67].

[39] J. Durnin, J. J. Miceli, Jr., and J. H. Eberly, Diffraction-Free Beams, Phys. Rev. Lett. **58**, 1499 (1987).

[40] H. Haug and S. W. Koch, *Quantum Theory of the Optical and Electronic Properties of Semiconductors: Fifth ed.* (World Scientific, Singapore, 2009).

[41] F. Wendler, A. Knorr, and E. Malic, Ultrafast carrier dynamics in Landau-quantized graphene, Nanophotonics **4**, 224 (2015).

[42] F. Wendler, A. Knorr, and E. Malic, Carrier multiplication in graphene under Landau quantization, Nat. Commun. **5**, 3703 (2014).

[43] D. W. Snoke, D. Braun, and M. Cardona, Carrier thermalization in Cu_2O: Phonon emission by excitons, Phys. Rev. B **44**, 2991 (1991).

[44] D. W. Snoke, W. W. Rühle, Y.-C. Lu, and E. Bauser, Evolution of a nonthermal electron energy distribution in GaAs, Phys. Rev. B **45**, 10979 (1992).

[45] P. Plochocka, P. Kossacki, A. Golnik, T. Kazimierczuk, C. Berger, W. A. de Heer, and M. Potemski, Slowing hot-carrier relaxation in graphene using a magnetic field, Phys. Rev. B **80**, 245415 (2009).

[46] M. Mittendorff, F. Wendler, E. Malic, A. Knorr, M. Orlita, M. Potemski, C. Berger, W. A. De Heer, H. Schneider, M. Helm *et al.*, Carrier dynamics in Landau-quantized graphene featuring strong Auger scattering, Nat. Phys. **11**, 75 (2015).

[47] S. A. Empedocles and M. G. Bawendi, Quantum-confined Stark effect in single CdSe nanocrystallite quantum dots, Science **278**, 2114 (1997).

[48] H. M. Price, T. Ozawa, and I. Carusotto, Quantum Mechanics with a Momentum-Space Artificial Magnetic Field, Phys. Rev. Lett. **113**, 190403 (2014).

[49] V. Lukose, R. Shankar, and G. Baskaran, Novel Electric Field Effects on Landau Levels in Graphene, Phys. Rev. Lett. **98**, 116802 (2007).

[50] N. Peres and E. V. Castro, Algebraic solution of a graphene layer in transverse electric and perpendicular magnetic fields, J. Phys.: Condens. Matter **19**, 406231 (2007).

[51] O. Gazzano, B. Cao, J. Hu, T. Huber, T. Grass, M. Gullans, D. Newell, M. Hafezi, and G. S. Solomon, Observation of chiral photocurrent transport in the quantum Hall regime in graphene, arXiv:1903.01487.

[52] S. O. Kasap, *Optoelectronics and Photonics* (Prentice Hall, Hoboken, NJ, 2001).

[53] S. M. Girvin, The quantum Hall effect: novel excitations and broken symmetries, in *Aspects Topologiques de la Physique en Basse Dimension. Topological Aspects of Low Dimensional Systems* (Springer, Berlin, 1999), pp. 53–175.

[54] N. R. Cooper and J. T. Chalker, Coulomb interactions and the integer quantum Hall effect: Screening and transport, Phys. Rev. B **48**, 4530 (1993).

[55] X. Cui, G.-H. Lee, Y. D. Kim, G. Arefe, P. Y. Huang, C.-H. Lee, D. A. Chenet, X. Zhang, L. Wang, F. Ye *et al.*, Multi-terminal transport measurements of MoS_2 using a van der Waals heterostructure device platform, Nat. Nanotechnol. **10**, 534 (2015).

[56] Z. Wu, S. Xu, H. Lu, A. Khamoshi, G.-B. Liu, T. Han, Y. Wu, J. Lin, G. Long, Y. He *et al.*, Even–odd layer-dependent magnetotransport of high-mobility Q-valley electrons in transition metal disulfides, Nat. Commun. **7**, 12955 (2016).

[57] R. Pisoni, A. Kormányos, M. Brooks, Z. Lei, P. Back, M. Eich, H. Overweg, Y. Lee, P. Rickhaus, K. Watanabe *et al.*, Interactions and Magnetotransport Through Spin-Valley Coupled Landau Levels in Monolayer MoS_2, Phys. Rev. Lett. **121**, 247701 (2018).

[58] I. Das, X. Lu, J. Herzog-Arbeitman, Z.-D. Song, K. Watanabe, T. Taniguchi, B. A. Bernevig, and D. K. Efetov, Symmetry-broken Chern insulators and Rashba-like Landau-level crossings in magic-angle bilayer graphene, Nat. Phys. **17**, 710 (2021).

[59] L. Wang, E.-M. Shih, A. Ghiotto, L. Xian, D. A. Rhodes, C. Tan, M. Claassen, D. M. Kennes, Y. Bai, B. Kim *et al.*,

Correlated electronic phases in twisted bilayer transition metal dichalcogenides, Nat. Mater. **19**, 861 (2020).

[60] C. Shen, Y. Chu, Q. Wu, N. Li, S. Wang, Y. Zhao, J. Tang, J. Liu, J. Tian, K. Watanabe *et al.*, Correlated states in twisted double bilayer graphene, Nat. Phys. **16**, 520 (2020).

[61] A. Picón, A. Benseny, J. Mompart, J. V. de Aldana, L. Plaja, G. F. Calvo, and L. Roso, Transferring orbital and spin angular momenta of light to atoms, New J. Phys. **12**, 083053 (2010).

[62] M. O. Scully and M. S. Zubairy, *Quantum Optics* (Cambridge University Press, Cambridge, 1997).

[63] S. Kim, J. Schwenk, D. Walkup, Y. Zeng, F. Ghahari, S. T. Le, M. R. Slot, J. Berwanger, S. R. Blankenship, K. Watanabe *et al.*, Edge channels of broken-symmetry quantum Hall states in graphene probed by atomic force microscopy, Nat. Commun. **12**, 2852 (2021).

[64] D. A. Abanin, P. A. Lee, and L. S. Levitov, Charge and spin transport at the quantum Hall edge of graphene, Solid State Commun. **143**, 77 (2007).

[65] D. B. Chklovskii, B. I. Shklovskii, and L. I. Glazman, Electrostatics of edge channels, Phys. Rev. B **46**, 4026 (1992).

[66] C. Gutiérrez, D. Walkup, F. Ghahari, C. Lewandowski, J. F. Rodriguez-Nieva, K. Watanabe, T. Taniguchi, L. S. Levitov, N. B. Zhitenev, and J. A. Stroscio, Interaction-driven quantum Hall wedding cake–like structures in graphene quantum dots, Science **361**, 789 (2018).

[67] A. Schiffrin, T. Paasch-Colberg, N. Karpowicz, V. Apalkov, D. Gerster, S. Mühlbrandt, M. Korbman, J. Reichert, M. Schultze, S. Holzner *et al.*, Optical-field-induced current in dielectrics, Nature (London) **493**, 70 (2013).